



Resolving the intertwining of inflammation and fibrosis in human heart failure at single-cell level

Man Rao^{1,2} · Xiliang Wang^{3,4} · Guangran Guo^{1,5} · Li Wang³ · Shi Chen¹ · Pengbin Yin² · Kai Chen¹ · Liang Chen¹ · Zemin Zhang^{3,6,7} · Xiao Chen¹ · Xueda Hu^{3,4} · Shengshou Hu¹ · Jiangping Song¹

Received: 5 January 2021 / Revised: 13 September 2021 / Accepted: 21 September 2021 / Published online: 3 October 2021
© Springer-Verlag GmbH Germany, part of Springer Nature 2021

Abstract

Inflammation and fibrosis are intertwined mechanisms fundamentally involved in heart failure. Detailed deciphering gene expression perturbations and cell–cell interactions of leukocytes and non-myocytes is required to understand cell-type-specific pathology in the failing human myocardium. To this end, we performed single-cell RNA sequencing and single T cell receptor sequencing of 200,615 cells in both human dilated cardiomyopathy (DCM) and ischemic cardiomyopathy (ICM) hearts. We sampled both lesion and mild-lesion tissues from each heart to sequentially capture cellular and molecular alterations to different extents of cardiac fibrosis. By which, left (lesion) and right ventricle (mild-lesion) for DCM hearts were harvest while infarcted (lesion) and non-infarcted area (mild-lesion) were dissected from ICM hearts. A novel transcription factor *AEBPI* was identified as a crucial cardiac fibrosis regulator in *ACTA2*⁺ myofibroblasts. Within fibrotic myocardium, an infiltration of a considerable number of leukocytes was witnessed, especially cytotoxic and exhausted CD8⁺ T cells and pro-inflammatory CD4⁺ T cells. Furthermore, a subset of tissue-resident macrophage, *CXCL8*^{hi}*CCR2*⁺*HLA-DR*^{hi} macrophage was particularly identified in severely fibrotic area, which interacted with activated endothelial cell via *DARC*, that potentially facilitate leukocyte recruitment and infiltration in human heart failure.

Keywords Single-cell sequencing · Heart failure · Inflammation · Fibrosis

Introduction

Heart failure (HF) is a chronic, progressive condition characterized by decreased cardiac systolic or diastolic function, resulting in insufficient blood supply to organs and tissues. HF remains a leading cause of morbidity and mortality,

affecting almost 24 million patients worldwide, and the 5-year mortality rate is approximately 50% [47]. The most prevalent etiologies are ischemic cardiomyopathy (ICM) and dilated cardiomyopathy (DCM). Effective treatments targeting the myocardium still require a detailed understanding of the biology of the failing heart.

The maintenance of cardiac homeostasis is finely tuned by many cell types in the myocardium. During the progression of

Man Rao, Xiliang Wang and Guangran Guo contributed equally to this work.

✉ Xueda Hu
hu_xue_da@pku.edu.cn

✉ Shengshou Hu
huss@fuwaihospital.org

✉ Jiangping Song
fwsongjiangping@126.com

¹ State Key Laboratory of Cardiovascular Disease, Fuwai Hospital, Chinese Academy of Medical Science, PUMC, 167 Beilishi Road, Xicheng District, Beijing 100037, China

² National Clinical Research Center for Orthopedics, Sports Medicine and Rehabilitation, General Hospital of Chinese PLA, Beijing 100039, China

³ BIOPIC and School of Life Sciences, Peking University, No. 5 Yiheyuan Road, Haidian District, Beijing 100871, China

⁴ Analytical Biosciences Limited, Beijing 100084, China

⁵ Department of Thoracic Surgery, Sun Yat-Sen University Cancer Center, Guangzhou 510060, China

⁶ Beijing Advanced Innovation Center for Genomics, Peking University, Beijing 100871, China

⁷ Peking-Tsinghua Center for Life Sciences, Peking University, Beijing 100871, China

HF, the heart undergoes complex remodeling-related processes such as cardiomyocyte (CM) cell death, fibrosis, and angiogenesis/neovascularization [39]. In particular, emerging evidence suggests that dysregulated inflammation in the heart plays an essential role in cardiac fibrosis, adverse cardiac remodeling and ultimately leads to HF [6]. Recent studies in small animals have shown that macrophages can promote cardiac fibrosis and diastolic dysfunction, and that T cells orchestrate cardiac fibrosis in nonischemic HF [23, 38]. Cardiac macrophage subsets in the diseased human hearts have recently been described [4], while other leukocyte subsets, such as lymphocytes, remain to be poorly characterized. Therefore, a comprehensive understanding of microenvironment alterations in the diseased heart would be a fundamental step towards identifying future therapeutics.

In recent years, single-cell RNA sequencing (scRNA-seq) analysis has significantly advanced our approach to study biological systems. At single-cell resolution, recent advances in mouse models have demonstrated unprecedented cell heterogeneity in mammalian hearts and cell type-specific regulators that can impact pathological cardiac remodeling [3, 13, 14, 19, 32, 49]. The scRNA-seq and single-nuclei RNA-sequencing (snRNA-seq) technology were also performed on human diseased and healthy hearts, mainly focusing on inter-cellular crosstalk between CMs and non-CMs [34, 51, 53]. However, the component of immune cells and their influence on late-stage human HF have not yet been fully characterized. In this study, we aimed to establish the single-cell landscape of non-CMs with a pronounced resolution in immune cells in failing human hearts with DCM and ICM. Moreover, we specifically sampled both ventricles from DCM, infarcted and non-infarcted myocardium from ICM left ventricle to further understand phenotypic alterations in severely fibrotic and inflamed heart. Hopefully, this comprehensive single-cell map of human heart failure with profound resolution in immune cell would pave path to finding effective immunotherapy in the near future.

Methods

Study approval

This study was approved by the Ethical Committee of Fuwai Hospital in Beijing, China. Written informed consent was obtained from all patients, and the experiments were performed in accordance with the approved study protocol.

Cardiac and blood cell isolation

Cardiac tissue samples were obtained from adult patients with DCM and ICM who were undergoing heart transplantation. Secondary causes leading to DCM were excluded

for patients enrolled in our study: cardiac amyloidosis, cardiac sarcoidosis, viral myocarditis, giant cell myocarditis, peripartum cardiomyopathy, chemotherapy-associated cardiomyopathy, obesity, diabetic cardiomyopathy, arterial coronary disease, valvular disease, and congenital heart disease. Briefly, upon excision, tissue samples were quickly immersed in ice-cold University of Wisconsin (UW) solution for transport to the laboratory. The epicardium and endocardium were removed. Then, we cut the tissue into 3 mm³ pieces and rinsed the fragments twice in cold PBS buffer. Then, cardiac cells were isolated by enzymatic digestion with a Neonatal Heart Dissociation Kit (Miltenyi Biotec, 130-098-373) for 56 min on a rotor at 37 °C according to the manufacturer's instructions. Enzymatic digestion was stopped by DMEM (Gibco, 11,995-065) supplemented with 10% fetal bovine serum (FBS, HyClone, SH30071). After centrifugation at 300 g for 5 min, the cell pellet was resuspended in red blood cell lysis buffer (Miltenyi Biotec, 130-094-183) and incubated on ice for 2 min to lyse red blood cells. In addition, blood was collected into EDTA-containing tubes, and the mononuclear cells were isolated by gradient centrifugation (HISTOPAQUE-1077, Sigma-Aldrich). The cell pellets were resuspended in sorting buffer (PBS supplemented with 2% FBS).

Flow cytometry and cell sorting

For the scRNA-seq experiment, the cell suspension was stained with BB515 mouse anti-human CD45 (BD, 5,64,585) at a concentration of 1:200 on ice in the dark for 30 min, and 7-AAD (BD, 5,59,925) was used to exclude dead cells. For scRNA-seq with TCR sequencing, the cell suspension was stained with eFluor[®] 450 anti-human CD3 (eBiosciences, 19,11,259) at 1:200 on ice in the dark for 30 min, as well as 7-AAD (BD, 5,59,925). Stained single-cell suspensions were washed with sorting buffer, and FACS sorting was performed on a FACSaria II cell sorter (BD Biosciences).

The anti-human antibodies used in other cell sorting experiments were as follows: APC-Cy7 mouse anti-human CD31 (BD, 5,63,653) at 1:400 and PE mouse anti-human DARC (BD, 5,66,424) at 1:400. Single cells from specific populations were collected for subsequent analysis by FACS sorting using a FACSaria II cell sorter (BD Biosciences), and data were analyzed with FlowJo software (Tree Star).

10× Genomics 3' single-cell RNA-seq

The FACS-sorted CD45⁺ and CD45⁻ single cells were processed through the Chromium[™] Single-Cell platform using Chromium[™] Single-Cell 3' Library and Gel Bead Kit

(10×Genomics) according to the manufacturer’s protocol. Briefly, 10,000~15,000 individual cells were sorted into PBS plus 2% FBS and loaded on the Chromium™ Single-Cell A Chip Kit (10×Genomics) according to the manufacturer’s protocol. The cells were then partitioned into Gel Beads in Emulsion in the Chromium instrument, where the cells and barcoded reverse transcription occurred, followed by amplification, fragmentation and 5’ adaptor, and sample index attachment. Libraries were sequenced on an Illumina HiSeqX system.

10× Genomics 5’ single-cell RNA-seq and TCR profiling

CD3⁺ cells from the LV of explanted hearts and corresponding peripheral blood were isolated by FACS separately. Single-cell 5’ transcriptome libraries were prepared with the Chromium™ Single-Cell 5’ Library kit. TCR-enriched libraries were prepared with the Chromium™ Single-Cell V(D)J Enrichment kit. Briefly, 10,000~15,000 individual T cells were loaded on a Chromium™ Single-Cell A Chip Kit (10×Genomics) following the manufacturer’s protocol. The cells were then partitioned into Gel Beads in Emulsion in the Chromium instrument. After reverse transcription, barcoded cDNAs were fragmented, end-repaired, ligated to adaptor and indexed as above. In addition, single-cell TCR sequences from the same individual cells were amplified from cDNA. Both transcriptome and TCR libraries were sequenced on an Illumina HiSeqX system.

Computational analysis of scRNA-seq data

Reads were mapped to the GRCh38 human genome (Ensembl 88, <http://asia.ensembl.org>) using the CellRanger toolkit (version 3.0.2, 10×Genomics) with the default parameters. Cells were discarded according to the following criteria: (1) cells that had fewer than 500 genes (UMI > 0); (2) cells that had fewer than 800 UMI or over 8000 UMI; and (3) cells that had more than 10% mitochondrial UMI counts. After the above quality control, adhering to the suggested integration workflow of Seurat V3 (version 3.1.1). To construct a reference, we identified “anchors” among batches. First, we split the combined object into a list using “SplitObject” function, with each donor as an element. Prior to finding anchors, we performed log-normalization and identified 2000 variable features individually for each with the “vst” method. Next, we identified anchors using the “FindIntegrationAnchors” function with default parameters. Here, we specified the normal datasets as a “reference”, with the remainder designated as “query” datasets. This approach substantially reduced computational time, particularly a

large number of datasets. We then integrated the batches using the anchors with the “IntegrateData” function with the “dims” parameter set to 30, which returns a Seurat object with a batch-corrected expression matrix for all cells. We then used this new integrated matrix for downstream analysis and visualization. We scaled the integrated data, setting the parameter “vars.to.regress” to “percent.mito” and “nCount_RNA”. Principal component analysis (PCA) was performed using the “RunPCA” function. The number of PCs was chosen by visualization plot with the ‘ElbowPlot’ function. A shared nearest neighbor (SNN) graph was constructed using the “FindNeighbors” function with the top 30 PCs, then cells were clustered by the “FindClusters” function with the ‘resolution’ parameter set to 0.5. The “RunUMAP” function was used for the visualization plot with the “umap-learn” method, setting “n.neighbors” to 40L, “dims” to 1:30, and “min.dist” to 0.3. Marker genes for each cluster were detected using the “FindAllMarkers” function, setting the parameter ‘min.pct’ to 0.3 and “logfc.threshold” to 0.6. Subsequently, cell clusters were annotated manually to the major cell types according to known markers. Any cluster with multiple markers of two types of cells was manually discarded as a doublet. A second round of clustering was performed on the B cells, CMs, endothelial cells (ECs), fibroblasts (FBs), myeloid cells, pericyte, smooth muscle cells (SMCs), and T/NK (namely, T and NK cell) populations, respectively. After grouping and separation using the “subset” command, and the above procedure was applied. For ECs, FB, myeloid cells and TNKs populations, the number of PCs used in the “FindNeighbors” function was 20, 15, 25, and 20, respectively. The “resolution” parameter of the “FindClusters” function was 0.5, 0.5, 0.5, 0.5, 0.5, 0.3, and 1.2. Any cluster with an extraordinarily high number of detected genes or UMI count was manually discarded as a doublet.

Differentially expressed genes ($p < 0.01$) were identified with the “FindMarkers” function of the Seurat package, setting “logfc.threshold” to 0.25, “min.pct” to 0.1, and “test.use” to the MAST method [16]. Gene symbols were first converted to Entrez gene IDs, while GO and KEGG pathway enrichment analysis ($p < 0.01$) was implemented using the clusterProfiler package (version 3.9.2).

We retrieved signature genes (neutrophil activation, interleukin-1 beta production, response to tumor necrosis factor, positive regulation of angiogenesis, arterial endothelial cell differentiation, endothelial cell proliferation, vasculogenesis, artery morphogenesis, extracellular matrix assembly, fibroblast proliferation, and cytotoxicity) from the GO database (GO:0,042,119, GO:0,032,611, GO:0,034,612, GO:0,045,766, GO:0,060,842, GO:0,001,935, GO:0,001,570, GO:0,048,844, GO:0,085,029, GO:0,048,144, and GO:0,019,835, respectively, <http://geneontology.org/>). The exhaustion score was calculated by the

mean expression values of *LAG3*, *TIGIT*, *PDCD1*, *HAVCR2*, and *CTLA4*. The pro-inflammatory scores were calculated by the mean expression values of *KLRD1*, *KLRC1*, *CXCR3*, *STAT3*, *IFNGR1*, and *HLA-B* [15], whereas the endothelium activation scores were calculated by the mean expression value of *DARC*, *SELE1*, *SELP*, *CSF3*, *RAB3C*, *IL33*, *CCL14*, *CX3CL1*, and *VWF* [36]. The signature score was computed by the Seurat function “AddModuleScore”.

RNA velocity analysis

The loom file representing the spliced and unspliced information of each sample was constructed by the velocity (version 0.17.17) python package based on the bam files from the Cell Ranger toolkit. After merging all the loom files, we separated cell clusters of interest. Data were normalized and scaled with the “SCTransform” function with the top 2000 HVGs. Clustering information was imported from the Seurat results, and the UMAP coordinates were rerun by the “RunUMAP” for visualization. RNA velocity values were calculated by the “RunVelocity” function of SeuratWrappers package, and visualization was performed by the “show.velocity.on.embedding.cor” function with the default parameter.

Cell–cell interaction analysis

The cell–cell interaction prediction was performed by CellPhoneDB (version 2.0) [52] using the log normalized expression data, setting the parameter “iterations” to 1000, “threshold” to 0.1, and “*p* value” to 0.05.

Developmental trajectory inference

We used the monocle R package (version 2.12.0). The cell clusters of interest were separated using the “subset” command of Seurat, and then a CellDataSet object was created with the “as.CellDataSet” function of monocle. After calculating size factors and estimating dispersions, differentially expressed genes among clusters along the trajectory were identified via the “differentialGeneTest” function. When determining significance, we set a *q* value threshold of 1E-100 for FB and 1E-80 for macrophages. We selected the top 800 genes ordered by *q* value for ECs and CD8⁺ T cells and the top 2000 genes for CD4⁺ T cells. Dimension reduction was performed by the “reduceDimension” function with the “DDRTree” method. After cell ordering, the “plot_cell_trajectory”, “plot_genes_in_pseudotime”, and “plot_genes_branched_heatmap” functions were used for visualization.

TCR analysis

We built a Cell Ranger V(D)J-compatible reference using the “mkvdjref” command with genes whose “gene_biotype” was annotated as “TR_C_gene”, “TR_D_gene”, “TR_J_gene” or “TR_V_gene” in the GRCh38 human genome. The “vdj” command of Cell Ranger was used to assemble TCR contigs and calculate their expression abundance in each library, setting “chain” to “TR”. We first selected the “high_confidence”, “productive” contigs and those UMIs ≥ 2 . Only in-frame TCR α – β pairs were considered to define the dominant TCR of a single cell. For cells with two or more α or β chains assembled, the α – β pair showing the highest read number was defined as the dominant α – β pair. Each unique dominant α – β pair was defined as a clonotype. If two or more cells had identical dominant α – β pairs, the dominant α – β pair was identified as a clonal TCR, and these T cells were identified as clonal T cells. To integrate the TCR results with scRNA-seq data, the TCR-based analysis was performed only for interesting cell clusters from the Seurat results. Cells with TCR information were analyzed using the STARTRAC R package (version 0.1.0) [56] with default parameters.

Regulatory analysis of transcription factors

To infer TF-target interactions, four software were included: the ARACNe-AP (ARACNe with Adaptive Partitioning) tool (version 1.4) [29], pySCENIC (version, 0.11.1), Dorothea (written in python), and CoRegNet package (version 1.20.0). ARACNe was run with the input of normalized expression values. First, the significance threshold for mutual information was calculated (*p* value $< 1E-8$), and thereafter, ARACNe ran 100 bootstraps to generate a consensus network that was robust to expression outliers with default parameters. The Pearson correlation coefficient was calculated with the “cor.test” function of R with normalized UMI counts. Raw expression matrix was adopted as input for SCENIC analysis [1]. The regulons and TF activities (AUCell) for each cell were calculated with motif collection version mc9nr. The significantly upregulated regulon was defined as log fold change more than 0.1 and adjusted *p* value $< 1E-5$. The normalized and log transformed data were obtained and TF activities was calculated according to Dorothea instruction. CoRegNet was implemented with default parameters with normalized expression matrix. The co-regulatory network was obtained by hLICORN function. Regulatory and cooperative evidence were used for gene regulatory network and co-regulatory network enrichment. All these

results were visualized with the complexheatmap and igraph package (version 1.2.4).

Immunofluorescence staining

Histological analysis was performed according to the standard protocols for paraffin-embedded samples. Embedded human myocardium samples were sectioned at a thickness of 5 μm . The sections were dewaxed in water for 45 min, and antigens were repaired in boiling EDTA solution in a pressure cooker. The antibodies used were as follows: DARC (Abcam, ab137044) at 1:400, CD31 (Abcam, ab9498) at 1:20, CXCL8 (Abcam, ab18672) at 1:100, S100A8/A9 complex (Abcam, ab22506) at 1:400, CD68 (Immunoway, PT-0054) at 1:100, Collagen-1 (Abcam, ab90395) at 1:100, and Periostin (Abcam, ab14041) at 1:400. The primary antibody was detected using biotin-conjugated anti-mouse or anti-rabbit secondary antibodies in conjunction with streptavidin horseradish peroxidase. The PerkinElmer Opal Multicolor IHC system was utilized to visualize antibody staining according to the manufacturer's protocol. Stained slides were scanned over the whole slide using the Vectra Polaris system (PerkinElmer), which initially captured the fluorescence spectra in five channels (DAPI, FITC, Cy3, Texas Red and Cy5).

Bulk RNA sequencing of human cardiac samples

Left ventricular tissues from explanted hearts ($n = 52$) and donor hearts ($n = 15$) were obtained. RNA was extracted using TRIzol (Thermo Fisher, 15,596–026) following the manufacturer's protocol, and subsequently, the RNA was quantified using a NanoDrop (Thermo Fisher). The quality of the RNA was evaluated with a fragment analyzer (AATI). All samples had an RNA integrity number greater than 7.0. Libraries were constructed in a strand-specific manner after depletion of rRNA. Briefly, rRNA depletion was performed with a Ribo-Zero™ Magnetic kit (Illumina, MRZG12324). RNA was reverse-transcribed into cDNA with reagents containing dUTP, and the ends containing "A" overhangs were polished and ligated with adaptors. Then, cDNA was sheared to an average size of 300–400 bp. The libraries were sequenced on an Illumina HiSeq X.

In vitro stimulation of DARC⁺ ECs and sequencing

DARC⁺ ECs were isolated by FACS from the LVs of explanted hearts. Cells were incubated in 0.1% gelatin-coated dishes with an endothelial cell medium complete kit (ScienCell, 1001). Human CXCL8 protein (R&D,

208-I-050) was added to stimulate DARC⁺ ECs at a final concentration of 8 ng/ml. Seventy-two hours after stimulation, the cells were harvested and washed twice with PBS.

RNA was extracted using an RNeasy Mini kit (QIAGEN, 74,104) by following the manufacturer's protocol. The concentration of RNA was quantified using a NanoDrop (Thermo Fisher), and the quality was evaluated with a fragment analyzer (AATI). Libraries were prepared with an NEBNext Poly(A) mRNA Magnetic Isolation Module kit (NEB) and an NEBNext Ultra RNA Library Prep Kit for Illumina Paired-end Multiplexed Sequencing Library (NEB). The libraries were sequenced on an Illumina Novaseq 6000.

Bulk RNA-seq data processing

Gene expression was quantified by RSEM with the same version of transcriptome annotation used for scRNA-seq data. TPM (transcripts per kilobase per million reads) were calculated by aggregating reads mapping to identical genes and then converting them to read counts implemented in the R function tximport. Differential gene expression was analyzed with DESeq2.

Data visualization and statistics

Microsoft R Open (version 3.6.1, <https://mran.microsoft.com/>) was used. The R packages ggplot2 (version 3.1.0), pheatmap (version 1.0.12) were used to generate graphs of the data. A false discovery rate (FDR) correction using Bonferroni procedure was applied jointly for all genes in the dataset.

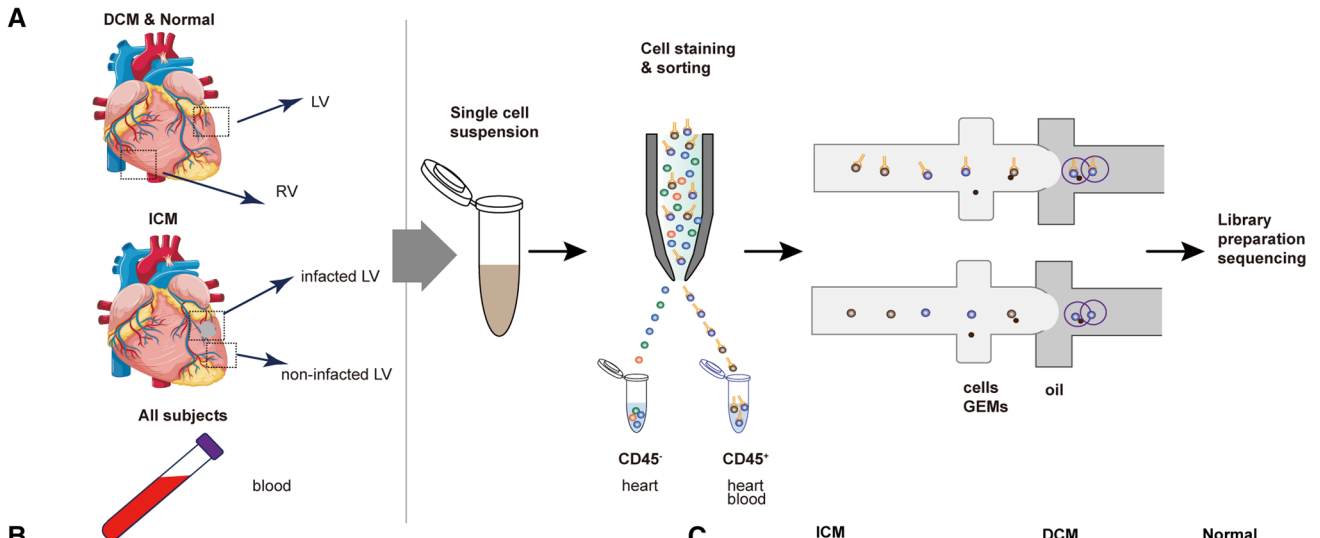
Data and code availability

The raw sequence data and processed expression matrix files have been deposited in the Gene Expression Omnibus under accession number GEO: GSE145154. Code and custom scripts for analyzing data are available upon request via Dr. Jiangping Song, fwsongjiangping@126.com.

Results

Major cell types in the human heart revealed by scRNA-seq

To understand gene express perturbation and generate a comprehensive cellular map of human failing heart at single-cell resolution, we included late-stage idiopathic DCM and ICM patients. As summarized in workflow: for



B

Patient	clinical information				Number of collected cells	
	Age	Sex	LVEF(%)	Tissue	CD45 ⁺	CD45 ⁻
DCM-1	58	Male	18	LV/RV/blood	4295/4096/5270	955/1901/-
DCM-2	60	Male	34	LV/RV/blood	5388/3969/7042	2436/1844/-
DCM-3	62	Male	18	LV/RV/blood	6119/6122/7767	3611/2652/-
ICM-1	40	Male	22	MI/NMI/blood	4633/4323/5335	2197/522/-
ICM-2	54	Male	30	MI/NMI/blood	3563/2716/5164	1998/2369/-
ICM-3	45	Male	30	MI/NMI/blood	4747/4206/7595	3582/1810/-
Normal-1	50	Male	65	LV/RV/blood	6544/5444/1903	5982/3026/-
Normal-2	53	Male	60	LV/RV/blood	7393/4262/1340	4933/6943/-

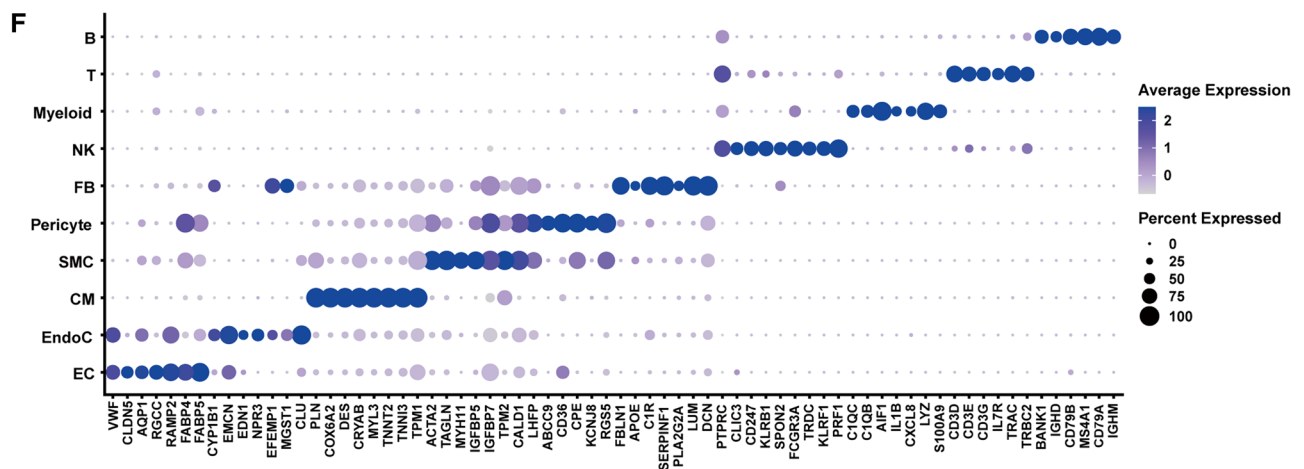
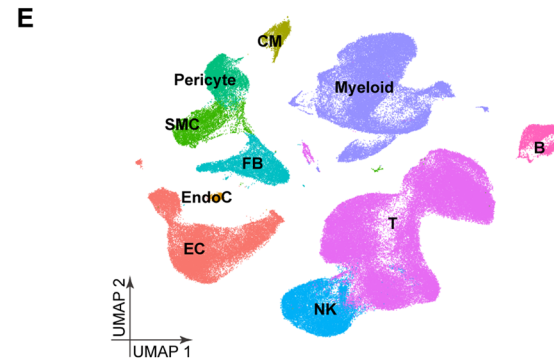
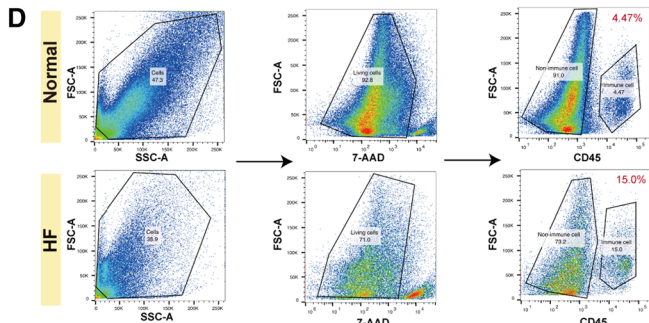
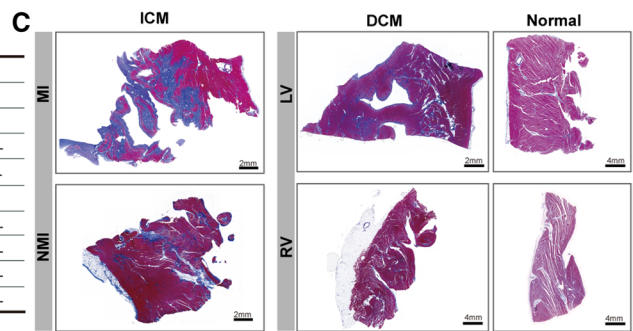


Fig. 1 Study design and the cellular landscape of human heart failure. **a** Workflow: for DCM and normal heart: left ventricle (LV) and right ventricle (RV) were dissected, whereas for ICM infarcted (MI) and non-infarcted myocardium (NMI) in LV were sampled. For each enrolled subject cardiac CD45⁻, cardiac CD45⁺ cells and blood CD45⁺ cells were sorted by FACS separately for scRNA-seq. **b** The enrolled subject baseline information and numbers of cell sequenced from each corresponding tissue. **c** Representative Masson staining of heart tissue samples enrolled in our study. **d** Representative FACS plots derived from a normal LV and a DCM LV. HF: heart failure. **e** UMAP plots showing major cell types found in heart and peripheral blood. EC: endothelial cell, EndoC: endocardial cell, SMC: smooth muscle cell, FB: fibroblast, CM: cardiomyocyte. **f** Dot-plot representing the signature gene expression in each major cell type. Circle size indicates the cell fraction expressing the signature gene and color indicates the gene expression level

DCM and nonfailing donor hearts, we dissected left ventricle (LV) and right ventricle (RV) myocardium. While for ICM hearts, the infarcted (MI) and non-infarcted (NMI) myocardium were sampled from LV (Fig. 1A). This sampling strategy was aimed to obtain differentially fibrotic and inflamed tissue within the same individual and, therefore, investigate genes deeply involved in cardiac fibrosis and inflammation. Moreover, DCM RV and ICM NMI would shed light on transcriptional profiles in less disease severity or remote remodeling region. In total, three DCM hearts, three ICM hearts and two nonfailing donor heart were subjected to droplet-based scRNA-seq (Fig. 1B). We outlined the baseline information and cell yield of enrolled subjects in Fig. 1B and Supp. Table 1.

As evident by pathological examination, DCM LV and ICM MI were found to be more fibrotic compared to DCM RV and ICM NMI, respectively (Fig. 1C). In each dissected myocardium, we isolated CD45⁻ cells and CD45⁺ cells separately by flow cytometry (FACS); additionally, we also isolated peripheral blood CD45⁺ cells from the same individual to track the CD45⁺ cell lineages in the myocardium. Further, the FACS data suggested an increase in CD45⁺ cell content in failing hearts compared to normal hearts (Fig. 1D).

A total of 40 samples from eight individuals were used for the scRNA-seq experiment, yielding a total of 165,999 cells after stringent quality-control filtering (see Methods, Fig. 1B, Fig.S1A). Clustering analysis revealed 13 major cell types, similar to recent studies [34, 51]. Based on canonical markers, the CD45⁻ cells included fibroblasts (FBs), endothelial cells (ECs), smooth muscle cells (SMCs), pericytes (PCs), endocardial cells and a small proportion of CMs, whereas the CD45⁺ cells included T cells, natural killer (NK) cells, B cells, and myeloid cells (monocytes, macrophages, dendritic cells, and mast cells) (Fig. 1E and Fig. S1B). All those cell types were detected in normal and failing hearts (Fig.S1C). The signature gene expression of each cell type also inferred robust cell clustering (Fig. 1F).

Most CMs could not be captured by 10X Genomics experiments due to their elongated shape and large size.

AEBP1 is a new cardiac fibrosis regulator that functions in activated fibroblasts and myofibroblasts

As cardiac fibroblasts (FBs) are a unique cell type of mesenchymal origin that provide the main source of extracellular matrix (ECM) production in cardiac fibrosis [18], we first investigated cellular composition in FBs. The FB lineage contained eight subsets: two resting FB subsets (C1 and C2), lipogenic FBs, collagen-processing FBs (COL-processing FBs), activated FBs, activated myofibroblasts (myoFBs), matrix myoFBs and contractile FB (Fig. 2A, B, and Supp. Table 2). Consistent with pathological examination, differentially expressed genes (DEG) analysis showed that pro-fibrogenic signatures (*POSTN*, *CTCF*, *AGT*, *COL1A2*, *COL1A2*, *COL3A1*, and *THY1*) were more pronounced in DCM LV and ICM MI when compared to DCM RV and ICM NMI, respectively (Fig. S2A). Matrix myoFB highly expressed different types of collagens was mainly found in ICM MI, resembling a subset structure-supporting FB found in fully matured fibrotic scar myocardium [18] (Fig. 2C, Fig.S2B). In addition, the matrix myoFBs, activated FBs and activated myoFBs showed highly concentrated ECM assembly properties (Fig. 2D). Furthermore, as the most pro-fibrotic population, activated myoFBs showed active proliferation features (Fig. 2D). Within normal heart, the C1 and C2 resting FBs were predominant with minimal ECM signatures (*POSTN* and *COL1A2*) (Fig. 2B, C). Lipogenic FBs highly expressed *DLK1*, which could suppress myoFB transition in mice, therefore, implying a potential fibrosis inhibition mechanism in HF and may explain its enrichment in DCM RV and ICM NMI [42] (Fig. S2B). Therefore, single-cell analysis showed FBs heterogeneity in terms of pro-fibrogenic signature, which is correlated with their spatial distribution.

To understand possible developmental connections among those FB subsets, we performed pseudo-time trajectory analysis. The transcription factor *AEBP1* was increasingly expressed in activated FBs and activated myoFBs (Fig. 2E), in correlation with the fibrotic markers *COL1A2* and *POSTN* (Fig. S2C). Furthermore, *AEBP1* showed highly expression in more fibrotic myocardium, through DEG analysis when compared DCM LV to RV, and ICM MI to NMI (Fig. S2A). This phenomenon was further supported by bulk RNA sequencing on LVs collected from 15 normal hearts and 52 failing hearts, *AEBP1* was notably upregulated in HF and its expression correlated with *POSTN* and *COL1A2* (Fig. 2F and Supp. Table 3). Further, the co-expression of *AEBP1* and *COL1A2* was also validated in Litvinukova

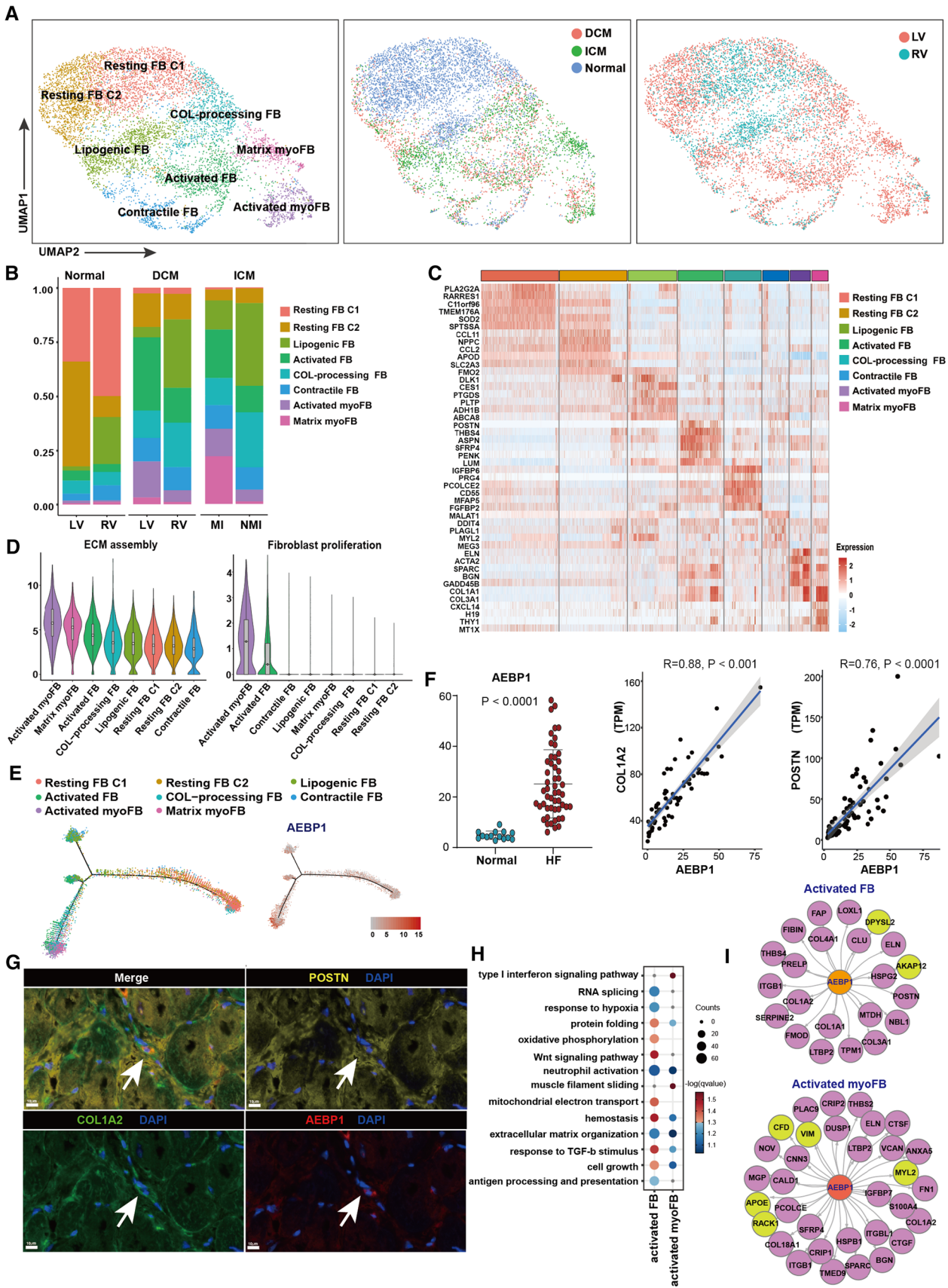


Fig. 2 Identifying fibroblast changes in human failing hearts. **a** UMAP plots of FB subsets, colored by disease (middle), and tissue location (right). **b** FB subset composition in normal, DCM and ICM hearts, separated by topographic regions. **c** Heatmap showing the differentially expressed genes of FB subsets. **d** GO enrichment analysis of FB subsets for fibrotic features. **e** Pseudo-time analysis of FB subsets and *AEBP1* expression plotted on the trajectory. **f** Bulk RNA sequencing (HF: $n=52$, normal: $n=15$) confirmed that *AEBP1* expression was significantly upregulated in failing hearts and strongly correlated with fibrotic markers. **g**. *AEBP1* expression was confirmed in fibrotic FBs in the human heart. **h** GO enrichment analysis of *AEBP1*-targeted genes in activated FBs and activated myoFBs. Circle size indicates the proportion of enriched gene in each functional term and color indicates FDR value for the enrichment score. **i** Network analysis showed *AEBP1*-co-expressed genes in activated FBs and activated myoFBs

et al. [34] data (Fig. S2D). We confirmed *AEBP1* expression within fibrotic cells in diseased hearts by immunostaining (Fig. 2G). Gene Ontology (GO) analysis of *AEBP1* co-expressed genes in activated FBs and activated myoFBs showed enrichment for ECM production and organization (Fig. 2H). Fibrotic genes such as *FAP*, *POSTN*, and *THBS4* and extracellular matrix genes including *VCAN*, *BGN*, *COL1A2*, and *ELN* were co-expressed with *AEBP1* and might serve as *AEBP1* targets in activated FB and activated myoFB, respectively (Fig. 2I). These results strongly indicate that *AEBP1* could be a new fibrosis regulator functioning via activated FB and activated myoFB in advanced HF.

An infiltration of dysfunctional CD8⁺ T cells and pro-inflammatory CD4⁺ T cells within lesion site accounts for cardiac inflammation.

Prior rodent-based study has suggested a crucial role of immune cells infiltration in cardiac fibrosis, especially in rodent cardiac injury models. However, less is known in human sample that how immune cells intervene with fibrosis and contribute to heart failure progression. We first assessed immune cells composition in normal and failing heart, from which T cells content was significantly higher in failing hearts (Fig. S3A, B). Our results demonstrated that the numbers of both CD4⁺ T cells and CD8⁺ T cells increased in the failing heart (Fig. S3B, C), and both CD4⁺ T cells and CD8⁺ T cells in DCM LV and ICM MI gained enhanced chemo-attractive and pro-inflammatory signature (Fig. S3D, E). Notably, *CD69*, a classical tissue-residency marker [28], was expressed in most cardiac T cells (Fig. S3F). In addition, T cells from peripheral blood showed distinct expression compared to heart (Fig. S3A, B). Therefore, the origination of cardiac T cells deserves more in-depth transcriptional analysis. We thereafter performed scRNA-seq with single-cell T cell receptor (TCR) VDJ sequencing

(scTCR-seq) on T cells sorted from the LV and peripheral blood collected from two additional DCM patients and one ICM patient (Fig. S3G, Supp. Table 1,4). ScTCR-seq would allow tracing T cell identity and identifying corresponding T cell transcriptional profile simultaneously. To comprehensively characterize the dynamic association among T cell subsets, we incorporated STARTRAC analysis to quantify the clonal expansion (expa), tissue migration (migr) and state transition (tran) of different T cell subsets [56].

Twenty-five subsets were annotated based on canonical markers and signature expression (Fig. 3A and Fig. S4A, B, Supp. Table 2). Among CD8⁺ T cells, we identified naïve (T_N), central memory (T_{CM}), effector memory (T_{EM}), effector (T_{EFF}), and recently activated effector (T_{EMRA}) subsets and a small population of exhausted CD8⁺ (T_{EX}) T cells exhibiting high expression of *PDCD1* and *LAG3* [54] (Fig. S4B and Supp. Table 2). CD8⁺ T_{CM} and CD8⁺ T_{EFF} cells were exclusively detected in the blood, while CD8⁺ T_{EMRA} and CD8⁺ T_{EX} cells were exclusively enriched in the myocardium (Fig. S4C). A descending cytotoxic signature (*NKG7*, *PRF1*, *GZMB*, *GNLY*) along with an increasing cell cycle arrest feature were observed with respect to CD8⁺ T_{EFF}, CD8⁺ T_{EMRA}, blood T_{EM}, T_{CM}, tissue T_{EM} and T_{EX} cells, consecutively (Fig. 3B). CD8⁺ T_{EFF} and CD8⁺ T_{EMRA} cells were highly proliferative and had strong STARTRAC migr scores, indicating that the effector CD8⁺ T cells actively migrated into the myocardium and expanded in the heart (Fig. 3C). Cells with identical TCRs could also illuminate the relationships between different T cell clusters, and the shared TCR usage implied CD8⁺ blood T_{EFF} experienced extensive state transition and developed into CD8⁺ T_{EMRA} cells in myocardium (Fig. 3D). The pairwise STARTRAC trans index quantitatively describes the developmental transition within T cells considering T cell clones defined by TCR sequence.

We could observe extensive and tight state transitions among CD8⁺ T_{CM}, blood CD8⁺ T_{EM}, CD8⁺ T_{EFF}, CD8⁺ T_{EMRA}, tissue CD8⁺ T_{EM} and CD8⁺ T_{EX} cells (Fig. 3E). To understand CD8⁺ T cell development, we constructed a pseudo-time trajectory of the aforementioned cell subsets (Fig. 3F). Together with RNA velocity, we observed that the CD8⁺ T_{EFF} population was activated, differentiated into CD8⁺ T_{EMRA} cells and further progressed into tissue CD8⁺ T_{EM} cells, which ultimately underwent exhaustion and gave rise to CD8⁺ T_{EX} cells (Fig. S4D). This observation was also validated by TCR clonal analysis (Fig. 3D). Resembling the CD8⁺ T cell exhaustion observed in cancer, the CD8⁺ T_{EX} population downregulated its cytotoxicity and proliferation ability and displayed extremely low state transition and migration capacity [56] (Fig. 3B, G). *NR4A1*, a transcription factor that was recently revealed to dominate the transcriptional profile of self-tolerant dysfunctional T cells [35], was upregulated along this path (Fig. S4E). Our findings provide

Fig. 3 Combined scRNA-seq and scTCR-seq of T cells in human failing hearts. **a** UMAP plots of T cells, split by tissue location (top, right) and disease (bottom, right). **b** Gene expression enrichment of selected functional terms for CD8⁺ T cells and CD4⁺ T cells. **c** STAR TRAC analysis of CD8⁺ T cells, showing the clonal expansion, tissue migration, and state transition abilities. **d** Developmental connection was validated by TCR clones for CD8⁺ T cells (CD8⁺ T_{EFF} and CD8⁺ T_{EMRA}) and CD4⁺ T cells (CD4⁺ T_{EM} and CD4⁺ T_{RM}). **e** Pairwise STARTRAC transition analysis of CD8⁺ T cell subsets, suggesting a potential correlation of CD8⁺ T_{EFF}, CD8⁺ T_{EMRA}, tissue CD8⁺ T_{EM}, and CD8⁺ T_{EX} cells. **f** Monocle result predicted CD8⁺ T cell trajectory. **g** Clonal expansion, migration, and transition potential of CD4⁺ T cells measured by STARTRAC analysis. **h** Relationship of CD4⁺ T_{EMRA}, CD4⁺ T_{CM}, CD4⁺ T_{EM}, and CD4⁺ T_{RM} subsets assessed by pairwise STARTRAC transition indices. **i** Monocle result showing the developmental origin of CD4⁺ T_{EM} cells

novel direct evidence that infiltrated cytotoxic CD8⁺ T cells lose their effector function and become exhausted in the failing heart.

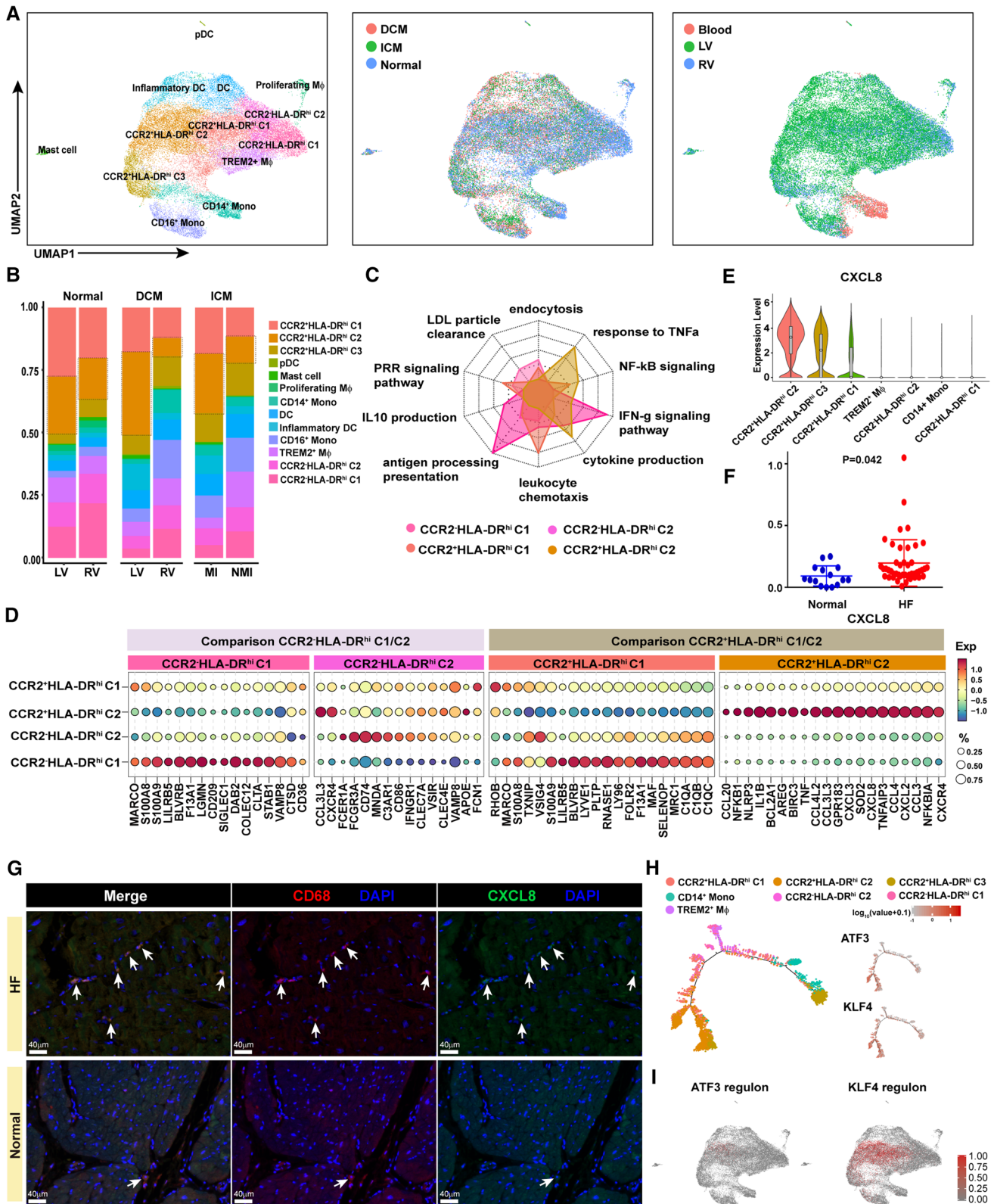
Within CD4⁺ T subsets, we detected CD4⁺ T_N, CD4⁺ T_{EFF}, CD4⁺ T_{CM}, CD4⁺ T_{EM}, and CD4⁺ T_{RM}, as well as two CD4⁺CD28^{low} T cell subsets with high expression of *GNLY* and *GZMH* [56] (Fig. S4B). CD4⁺ T_N, CD4⁺ T_{EFF}, and CD4⁺ T_{CM} cells predominantly emerged in the blood, while CD4⁺ T_{EM} and CD4⁺ T_{RM} cells were exclusively enriched in the myocardium (Fig. S4C). As a group of IFN-γ producing cells, the CD4⁺ T_{EM} cells had a strong pro-inflammatory signature [15] (Fig. 3B and Fig. S4B). The CD4⁺ T_{RM} cells specifically expressed the tissue repair-promoting protein *AREG* [31] (Fig. S4B). Two subsets of CD4⁺CD28^{low} T cells were specifically enriched in ICM (Fig. 3A). These two subsets are well known for their pro-inflammatory functions and their ability to kill ECs in vitro, and, therefore, likely contribute to coronary artery disease [37]. The CD4⁺CD28^{low} T cells showed an inter-tissue distribution, with high expression of the tissue-shuttling genes *SIPR1* and *ITGB7* [46, 56] (Fig. S4B). The observation that they had the highest STARTRAC migr score among CD4⁺ T cells also confirmed this feature (Fig. 3G). The pairwise STARTRAC tran index illustrated that CD4⁺CD28^{low} T cells experienced a possible transition with CD4⁺ T_{EM} (Fig. 3H). The trajectory and velocity analysis confirmed that the CD4⁺CD28^{low} T cells and pro-repair CD4⁺ T_{RM} cells independently transitioned to less cytotoxic but pro-inflammatory CD4⁺ T_{EM} cells, which led to the final state in the failing heart (Fig. 3I and Fig. S4F). The identical T cell clones across CD4⁺ T cell clusters also verified their state connections (Fig. 3D). Previously reported transcription factors, such as *BATF* [8], *BHLHE40* and *RBPJ* [56], were upregulated during the development of pro-inflammatory CD4⁺ T cells (Fig. S4E). Therefore, we speculated that since the cytotoxicity of massive infiltrated CD8⁺ T was alleviated in failing hearts, preventing CD4⁺ T cells pro-inflammatory transition would be a favorable and effective anti-fibrosis direction.

CCR2⁺HLA-DR^{hi} macrophages are major tissue-resident immune cells promoting inflammation in failing hearts

scTCR-seq analysis revealed majority pro-inflammatory T cells were infiltrated from blood, according to established work, cardiac tissue-resident populations mainly involved macrophages played essential roles in lymphocyte recruitment and cardiac fibrosis. We next examined myeloid cells in our dataset, clustering of myeloid cells identified 13 clusters: *CD14*⁺ monocytes (mono), *CD16*⁺ mono, dendritic cells (DCs), inflammatory DCs, plasmacytoid DCs, mast cells, and macrophages (Fig. 4A and Supp. Table 2.). The canonical marker for each subset was plotted on UMAP reflected minimal cell contamination (Fig. S5A).

We first compared the transcriptional profiles of macrophages among three groups: failing and normal hearts, LV and RV of DCM, MI, and NMI in ICM, respectively. The shared regulation may highlight the common pathway in cardiac fibrosis and inflammation. We found that in more fibrotic counterpart, highly expressed genes were prone to enrich in leukocyte chemotaxis (*CXCR4*, *CXCL8*, *CXCL2*, and *IL1B*), antigen processing and presentation (*HLA-DRA* and *HLA-DRB1*) and cytokine secretion (*NLRP3*, *EGR1*, and *BIRC3*) (Fig. S5B and Supp. Table 5). On the contrary, normal heart or less fibrotic myocardium had more pronounced expression in homeostasis-related terms such as cell respiration, endocytosis, LDL particle clearance and pattern recognition receptor signaling pathway (Fig. S5B and Supp. Table 5). Both DCM LV and ICM MI showed more pronounced genes expression on hemopoiesis and chemoattractant compared to DCM RV and ICM NMI, respectively (Fig. S5B, Supp. Table 5). Therefore, our result reflected macrophages enriched in severely fibrotic region could activate NF-β signaling, facilitate hemopoiesis and leukocyte recruitment and thereafter promote adverse cardiac remodeling including cardiomyocyte death, fibrosis and inflammation in heart failure, in accordance with previous works [4, 44].

Insights from lineage tracing mice have demonstrated that macrophages of different origin selectively orchestrated distinct tissue responses [3, 13]. In our data macrophages can be further divided into different subsets by *CCR2* and MHC class II molecule expression [4]: *CCR2*⁻*HLA-DR*^{hi} and *CCR2*⁺*HLA-DR*^{hi} macrophages. Additionally, we identified a novel *TREM2*⁺ subset with a signature similar to that of murine aortic *TREM2*⁺ macrophages [11] (Fig. S5C,D). The expression of *LYVE1* [4], *VSIG4* [30], and *FOLR2* [34] identified the *CCR2*⁻*HLA-DR*^{hi}, *CCR2*⁺*HLA-DR*^{hi} C1, *CCR2*⁺*HLA-DR*^{hi} C2, and *TREM2*⁺ Mφ clusters as tissue-resident populations whereas *CCR2*⁺*HLA-DR*^{hi} C3 was likely newly infiltrated subset (Fig. S5C, D).



Since previous study in human heart only described *CCR2*⁻ and *CCR2*⁺ macrophage, little is known in their subpopulation emerged in healthy and diseased heart. In

diseased heart, *CCR2*⁻*HLA-DR*^{hi} C1/C2 tended to enrich in DCM RV and ICM NMI, whereas *CCR2*⁺*HLA-DR*^{hi} C1/C2 preferentially distributed in DCM LV and ICM MI

Fig. 4 Diversity of myeloid cells in human failing hearts. **a** UMAP plots of myeloid subsets, colored by disease (middle), and tissue location (right). **b** Comparison of macrophages in HF/normal heart (top left), DCM LV/RV (top right) and ICM MI/NMI (bottom left). **c** Radar plot showed GO enrichment of highly expressed genes in different tissue-resident macrophages subsets. **d** Dot-plot showed differentially expressed genes in different tissue-resident macrophages subsets. Top bar indicated comparison groups. **e** Violin plots of *CXCL8* expression in macrophages. **f** Bulk RNA-seq showed that *CXCL8* expression was significantly upregulated in failing hearts (HF: $n=52$, normal $n=15$). **g** The presence of *CXCL8*⁺ macrophages in the failing heart (upper) and the normal heart (lower) was validated by immunostaining. **h** Macrophage development in failing hearts and the expression of transcription factors were plotted on trajectory maps. **i** SCENIC analysis indicated the regulon of *ATF3* and *KLF4* was switched on in *CCR2*⁺*HLA-DR*^{hi} C2 macrophages

(Fig. 4B). Consequently, we performed DEG analysis for *CCR2*⁺*HLA-DR*^{hi} C1/C2 and *CCR2*⁻*HLA-DR*^{hi} C1/C2 separately. The *CCR2*⁻*HLA-DR*^{hi} C1 displayed highly expression of genes involved in negative immunomodulation (*LILRB5*, *MAF*, *SIGLEC1*), tissue-residency (*LYVE1*) and homeostasis (*SLC40A1*, *BLVRB*, *STAB1*, *DAB2*) while pattern recognition receptors (*CLEC4E*, *CLEC7A*, and *CLEC10A*) were upregulated in *CCR2*⁻*HLA-DR*^{hi} C2 (Fig. 4C, D and Supp. Table 5). Correspondingly, *CCR2*⁺*HLA-DR*^{hi} C1 showed high phagocytosis facilitators (*CIQA* and *CIQB*) but *CCR2*⁺*HLA-DR*^{hi} C2 actively expressed key components in NLRP3 inflammasome and NF- κ B signaling (Fig. 4C, D). The DEG analysis reflected that *CCR2*⁻*HLA-DR*^{hi} C2 and *CCR2*⁺*HLA-DR*^{hi} C2 were likely a pro-inflammatory status compared to *CCR2*⁻*HLA-DR*^{hi} C1 and *CCR2*⁺*HLA-DR*^{hi} C1, respectively. Notably, the pro-angiogenic chemokine *CXCL8* was upregulated in *CCR2*⁺*HLA-DR*^{hi} C2 cells, particularly highly expressed in DCM LV and ICM MI (Fig. 4D, E). The increased expression of *CXCL8* was verified by bulk RNA sequencing (52 HF and 15 normal hearts) (Fig. 4F and Supp. Table 3). The enrichment of *CXCL8*⁺ macrophages in failing heart was further confirmed by immunostaining (Fig. 4G). Taken together, our data suggested that *CCR2*⁺*HLA-DR*^{hi} macrophages play a pro-inflammatory role in failing hearts.

The *TREM2*⁺ M ϕ subset that we characterized in the failing heart was previously reported in adipose tissue and brain as a disease-associated tissue-resident macrophage population [25, 26] (Fig. S5C). The specific expression of *SPP1* and *LGALS3* (Fig. S5C) suggested that *TREM2*⁺ M ϕ may influence angiogenesis and immune suppression [25], play a protective role under stress. Functional analysis showed that *TREM2*⁺ M ϕ may represent an intermediate status with a compromised inflammatory response and phagocytosis compared to *CCR2*⁻*HLA-DR*^{hi} and *CCR2*⁺*HLA-DR*^{hi} tissue-resident macrophages (Fig. S5E).

We further investigated the developmental connection of macrophages in failing hearts. Monocle analysis showed that both *CCR2*⁺*HLA-DR*^{hi} C3 (the right branch) and *TREM2*⁺

M ϕ (the middle branch) could potentially link with tissue-resident subsets: *CCR2*⁺*HLA-DR*^{hi} C2 (Fig. 4H). The RNA velocity results also confirmed that both *TREM2*⁺ M ϕ and *CCR2*⁺*HLA-DR*^{hi} C3 show directional flow towards *CCR2*⁺*HLA-DR*^{hi} tissue-resident subsets, suggesting that *CCR2*⁺*HLA-DR*^{hi} tissue-resident macrophages might arise from both infiltrated *CCR2*⁺*HLA-DR*^{hi} C3 and *TREM2*⁺ M ϕ rather than *CCR2*⁻*HLA-DR*^{hi} macrophages in silico (Fig. S5F). The transcription factors *ATF3* [12] and *KLF4* [33], which were reported to be involved in macrophage differentiation, might promote the transition from *CCR2*⁺*HLA-DR*^{hi} C3 into *CCR2*⁺*HLA-DR*^{hi} C2 (Fig. 4H). Indeed, single-cell regulatory network inference and clustering (SCENIC) analysis also indicated the *ATF3* and *KLF4* regulon were on in *CCR2*⁺*HLA-DR*^{hi} C2 (Fig. 4I and Fig. S5G). All the analysis above supports the notion that *CXCL8*^{hi}*CCR2*⁺*HLA-DR*^{hi} macrophage, might arise from both infiltrated *CCR2*⁺*HLA-DR*^{hi} C3 and *TREM2*⁺ M ϕ play a distinctive pro-inflammatory role in failing hearts.

EC remodeling is witnessed and activated EC with leukocyte recruitment potential is enriched in severely fibrotic myocardium

As a central cellular component of the human myocardium, ECs regulate leukocyte infiltration and thereby local inflammation [50], in addition to angiogenesis and neovascularization during tissue remodeling [27]. We found that vascular ECs were the most prevalent EC lineage, while lymphatic ECs accounted for only a small fraction (Fig. 5A). In diseased heart, activated EC was enriched in DCM LV and ICM MI comparing to DCM RV and ICM NMI (Fig. S6A). The *CD36* and *AQP1* implied active metabolic status (Fig. S6B, C) [40]. The pseudo-time analysis inferred that activated EC exhibited unique cell fate (Fig. 5B). The chemotactic cytokine *CCL14* [9], the Duffy antigen receptor for chemokines *DARC* and the endothelial-leukocyte adhesion molecule *SELE* were specifically expressed in activated ECs, in accordance with the Litvinokova et al.'s report (Fig. 5B and Fig. S6C) [34]. The activated ECs had a significant endothelium activation signature [36] (Fig. 5C), and the transcription factors *NR2F2* and *CEBPD* associated with this EC subset (Fig. 5B). *NR2F2* is the master regulator that induces venous fate and antagonizes arterial fate [55], whereas *CEBPD* participates in activating the transcription of various inflammatory genes [5]. In addition, cell adhesion molecules involved in leukocyte recruitment (*VCAM1*, *SELE*, *SELP*) were closely co-expressed with *NR2F2* (Fig. 5B and Fig. S6C), highlighting the leukocyte recruitment potential of this subset. Further, we validated that activated EC accounted for a subset vessel in failing heart by immunofluorescence (Fig. 5D).

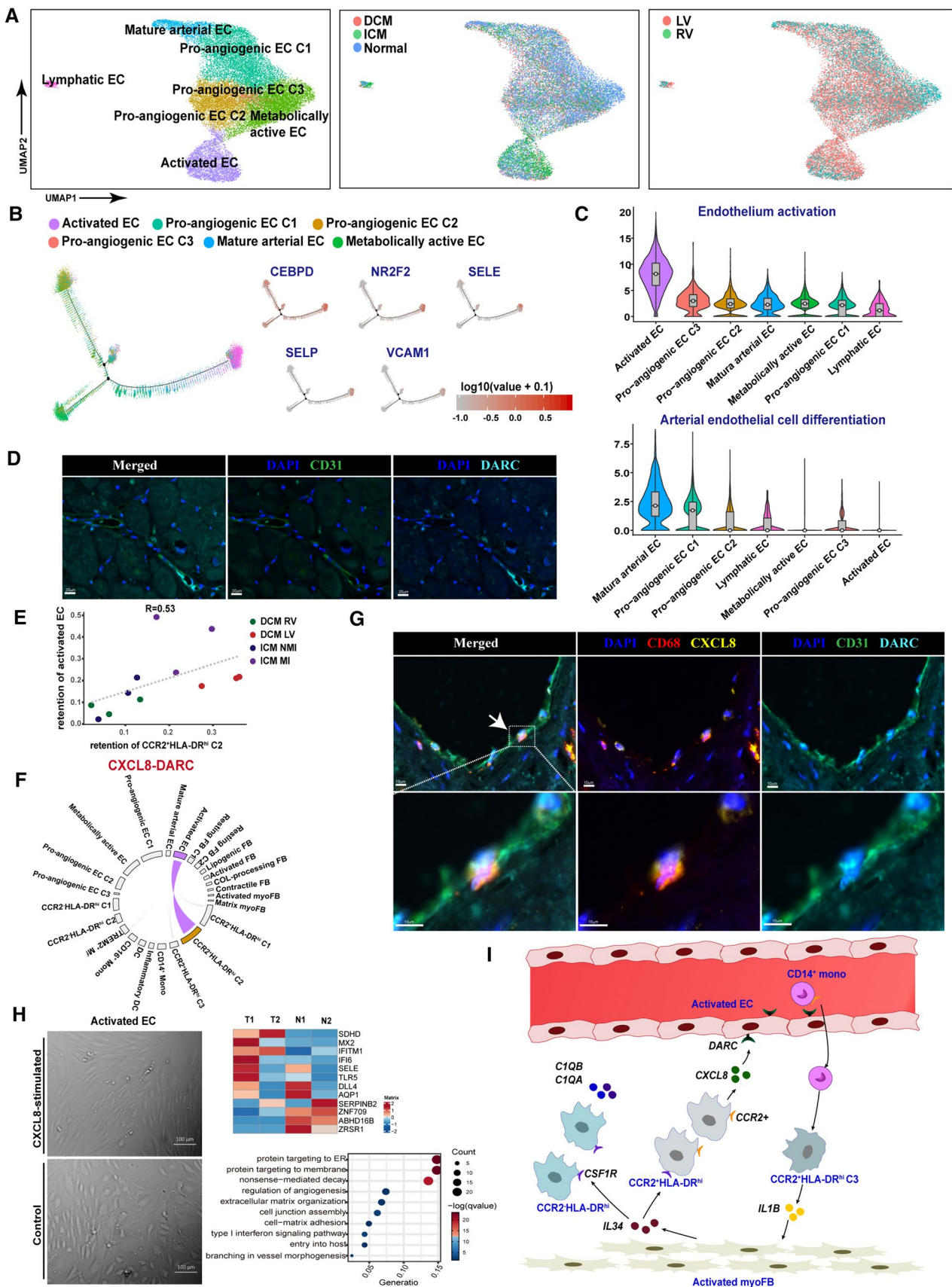


Fig. 5 Endothelial cells remodeling and interaction with *CXCL8*+ macrophages further promoted inflammation in human failing hearts. **a** UMAP plots of EC subsets, colored by disease (middle) and tissue location (right). **b** Pseudo-time relationship of EC subsets and expression of genes involved in leukocyte recruitment on trajectory map. **c** GO enrichments of selected functions in EC subsets. **d** Immunostaining validated the subset of *DARC*⁺ EC. **e** Correlation of the *CCR2*⁺*HLA-DR*^{hi} C2 and the activated EC retention in each sample. **f** Circos plots showing the predicted cell–cell interactions mediated by *CXCL8* and *DARC*. The expression of the *CXCL8-DARC* pair is highlighted in purple. **g** Multicolor IHC staining of *DARC*⁺ ECs and *CXCL8*⁺ macrophages confirmed juxtaposition in the failing heart. **h** Snapshot of *CXCL8*-stimulated activated ECs and non-stimulated activated ECs (left), heatmap of differentially expressed genes between the two groups and the GO enrichment of differentially expressed genes. T1 and T2: stimulated activated ECs derived from two patients, N1 and N2: non-stimulated activated ECs derived from the two patients. **i** Schematic representation of predicted cell–cell interactions in the failing hearts. *CXCL8-DARC* interaction could potentially facilitate monocyte recruitment and subsequent fibroblast activation. This will ultimately exacerbate cardiac inflammation in the failing heart

Other functional EC groups present in our data were pro-angiogenic ECs, consistent with the observation in mouse ischemic injury (Fig. 5A) [32]. We could identify three subsets: (i) pro-angiogenic EC C1 cells, which highly expressed *HEY1* and might mediate arterial cell fate decisions and pro-angiogenic effects in mammals [17, 21] (Fig. 5C and Fig. S6D); (ii) pro-angiogenic EC C2 cells, which were characterized by a sprouting signature; and (iii) pro-angiogenic EC C3 cells having a specific expression on *TNFRSF4*, suggesting its potential interaction with T cells (Fig. S6C, D) [24]. Our results revealed complex cellular composition of the EC lineage. To further investigate EC remodeling associated with fibrosis, and compare ECs derived from DCM LV and ICM MI with DCM RV and ICM NMI, respectively, we detected genes involved in response to ROS, chemokine, IFN- and TNF were activated within more fibrotic myocardium (Fig. S6E). These results indicated that endothelium inflammation, particularly in activated EC was also strongly associated with fibrosis.

***CXCL8*^{hi}*CCR2*⁺*HLA-DR*^{hi} macrophage interacts with activated endothelial cell via *DARC*, which potentially facilitate leukocyte recruitment and infiltration in heart failure.**

Complex cell crosstalk orchestrated adverse cardiac remodeling, however, details in cellular communications in failing heart are yet to be unraveled. As such, to investigate the rewiring of cell–cell interactions during HF, we mapped receptor–ligand pairs onto cell subsets to construct a putative cell interaction network by CellPhoneDB [52] and summarized interacting ligand–receptor pairs in Supp. Table 6. Knowing that DCM LV and ICM MI were more fibrotic than DCM RV and ICM NMI, respectively, we characterized

highly expressed receptor–ligand pairs expressed by the cell subsets that were preferential distributed in DCM LV and ICM MI. Subsequently, we observed a strong correlation between the proportion of *CCR2*⁺*HLA-DR*^{hi} C2 cells in each sample and the proportion of activated ECs (Fig. 5E), potentially reflecting their functional connection. The cell–cell interaction analysis found that *CXCL8-DARC* was among top interacting pair between *CCR2*⁺*HLA-DR*^{hi} C2 cells and activated EC (Supp. Table 6). Aforementioned analysis demonstrated that *CCR2*⁺*HLA-DR*^{hi} C2 cells highly expressed *CXCL8*, while its receptor *DARC* was expressed in activated ECs (Fig. 5F). Multicolor IHC staining of both DCM and ICM heart tissues confirmed the physical juxtaposition of *CXCL8*-expressing macrophages and *DARC*-expressing ECs (Fig. 5G). We then isolated activated ECs from explanted hearts and exposed them to *CXCL8* for 72 h. *CXCL8*-stimulated activated ECs transformed from a cobble stone-shaped into an elongated shape, upregulated genes involved in cell adhesion and leukocyte infiltration were determined by bulk RNA-seq. Upon stimulation, the function of highly expressed genes mainly associated with the type I interferon signaling pathway, regulation of angiogenesis and cell–matrix adhesion (Fig. 5H). These results further supported that *CXCL8* could activate endothelium and potentially enhance leukocyte infiltration (Fig. 5I).

Discussion

Inflammation and cardiac fibrosis are known to play crucial roles in HF [2]. Previous preclinical studies provided promising approaches targeting interactions of the immune and stromal cells in HF [22, 38], however, the failure of related clinical trials [10] highlighted that a comprehensive understanding of the complex microenvironment in the failing human heart is of great importance. Fine mapping the landscape in diseased heart tissue at single-cell resolution facilitate the identification of effective cell-type-specific drug targets. In this scRNA-seq study, we purposely sampled differentially fibrotic myocardium to reveal the shared mechanisms that DCM and ICM adopted to develop fibrosis and inflammation. Hence our study generated a valuable resource for HF therapeutic navigation regardless of the cause. Although lack of further experimental validation, we suggested that transcription factor *AEBP1* was a strong candidate for a novel cardiac fibrosis regulator specifically expressed in activated fibroblasts and myofibroblasts. Additionally, *AEBP1* loss-of-function could lead to deficiency in collagen assembly and the knock-out mouse model further support the potential role in cardiac fibrosis [7].

Meanwhile, T cell infiltration has been proposed to facilitate cardiac fibrosis, however, the origin and function of infiltrated T cell in human heart failure was not clearly

defined. Our study demonstrated the dynamic change of different T cell subset at an unprecedented depth with state-of-the-art technology. Among infiltrated massive lymphocytes in failing heart, CD8⁺ T cells undergo exhaustion in the failing human heart. Considering that at least some CD8⁺ T cells could be autoreactive, in contrast to the role of CD8⁺ T cells in cancer [54], CD8⁺ T cell exhaustion might be regarded as beneficial to the heart. With lineage tracing, we confirmed that recruited CD4⁺CD28^{low} T cells and tissue-resident CD4⁺ T_{RM} cells experienced extensive transition towards a pro-inflammatory Th1-like status in HF, therefore, preventing *BATF/RBPJ*-mediated CD4⁺ T cell transition may constitute a novel and promising therapeutic strategy. The tissue-resident *CCR2⁺HLA-DR^{hi}* macrophages, activated ECs and activated myoFBs were synergistically enriched in DCM LV and ICM MI. Together with infiltrated T cells, our results demonstrated that both the tissue-resident and infiltrated immune cell population orchestrated inflammation in the failing heart.

The concomitant enrichment of different cell types in severely fibrotic myocardium suggested those cellular communications likely contributing to disease progression. With the known roles and our analysis, thus it is rational to conclude *CCR2⁺HLA-DR^{hi}* macrophages were tightly connected with fibrosis and cardiac inflammation. Meanwhile, *DARC⁺* ECs were also enriched in inflamed ileum and fibrotic liver, cell migration assay confirmed activated endothelium facilitated monocyte infiltration [36, 41]. However, the detailed molecular stimulus was not previously identified. Inference of cell–cell interaction identified a possible underlying mechanism for sustained inflammation that CXCL8-stimulated *DARC⁺* ECs upregulate cell adhesion molecules to facilitate leukocyte infiltration. Indeed, three cognate receptors were known for *CXCL8*, *CXCR1*, *CXCR2*, and *DARC*, however, *CXCR1/CXCR2* expression were hardly detectable in our dataset (Fig.S7). Therefore, we reasonably presumed in failing heart *DARC* was the main receptor interacting with *CXCL8*.

CXCL8 is almost undetectable in unstimulated cells and could be significantly upregulated by cellular stress [20]. Intriguingly, *CXCL8* was not expressed in rodents, therefore, this study highlights importance of human sample-based discovery. Although *CXCL8* was reported to be expressed by various cells, minimal *CXCL8* expression was found in other but *CCR2⁺HLA-DR^{hi}* macrophages, reflecting that *CCR2⁺HLA-DR^{hi}* macrophages were the major source for *CXCL8* production in human failing heart. Clinical studies revealed that *CXCL8* level in acute ST-segment elevation myocardial infarction patients' blood was positively associated with infarct size and LV dysfunction, indicating *CXCL8* may facilitate HF progression [48]. A recent study demonstrated that *CXCL8* associated elevated levels of neutrophil/monocyte and worse prognosis in cancers, supporting

CXCL8 could promote immune cell infiltration [45]. An anti-*CXCL8* monoclonal antibody is in a Phase II trial for treating chronic obstructive pulmonary disease and rheumatoid arthritis [43]. Considering its upregulation in macrophages during HF, inhibiting *CXCL8* may be a potential novel approach for suppressing inflammation in the failing myocardium.

Conclusions

This study provides the first single-cell transcriptome atlas of leukocytes and non-myocytes in the failing adult human heart. Beyond providing reference information as a resource, we report on interaction networks that may stimulate a multitude of further mechanistic studies. Here, we highlight our major findings: (1) Fibroblasts underwent extensive phenotypic remodeling in human failing heart, *AEBP1* could be a novel cardiac fibrosis regulator mainly functions in *POSTN⁺* fibroblast and *ACTA2⁺* myofibroblast. (2) Massive cytotoxic CD8⁺ and pro-inflammatory CD4⁺ infiltrated into failing heart, however, CD8⁺ T would ultimately become exhausted and CD4⁺ T would transit into a more inflammatory status. (3) As major tissue-resident immune cells, a subset of *CXCL8^{hi}CCR2⁺HLA-DR^{hi}* macrophages preferentially locate in severely fibrotic myocardium and facilitate leukocytes recruitment and inflammation. (4) A unique subset of *DARC⁺* EC associates with cardiac fibrosis and would interact with *CXCL8^{hi}CCR2⁺HLA-DR^{hi}* macrophages in human heart failure. This crosstalk could potentially facilitate leukocyte infiltration, aggravate sustained cardiac inflammation and further deteriorate cardiac function. A major limitation of our study is that particular cell subsets and conclusions derived from cell state transition analysis need further experimental validation, for instance, using animal models to recapitulate the cell lineage development. Such confirmed findings may ultimately help to implement novel therapeutic approaches for the treatment of myocardial remodeling in ischemic and nonischemic HF patients.

Supplementary Information The online version contains supplementary material available at <https://doi.org/10.1007/s00395-021-00897-1>.

Acknowledgements We sincerely acknowledge Dr. Ulrich Hofmann at University Clinic Halle (Germany) and Dr. Maarten Hulsmans at Harvard Medical School for their tremendous contribution to this project. We thank Li Yang, Rui Yang, Fei Wang, Jian Meng and the BIOPIC FACS facility for technical help.

Author contributions MR, GG, XH, SH, and JS designed the study, XH, SH, and JS supervised the study. MR, GG, LW, and XH performed the experiment. XW, MR, GG, and XH analyzed the data. GG and SC collected clinical samples and clinical data. MR, PY, XW, GG, and XH wrote the manuscript. ZZ, PY, XH, SH, and JS made revisions.

XH, SH, and JS provided funding. All authors read the manuscript and approved it before submission.

Funding This work is supported by the R&D Program of Beijing Municipal Education commission (KJZD20191002301), CAMS Initiative for Innovative Medicine (2017-I2M-003, 2016-I2M-015), the National Natural Science Foundation of China (31601063), SLS-Qidong Innovation Fund and Beijing Advanced Innovation Centre for Genomics at Peking University.

Declarations

Conflict of interest The authors declared that they have no conflict of interest.

References

- Aibar S, González-Blas CB, Moerman T, Huynh-Thu VA, Imrichova H, Hulselmans G, Rambow F, Marine JC, Geurts P, Aerts J, van den Oord J, Atak ZK, Wouters J, Aerts S (2017) SCENIC: single-cell regulatory network inference and clustering. *Nat Methods* 14:1083–1086. <https://doi.org/10.1038/nmeth.4463>
- Bacmeister L, Schwarzl M, Warnke S, Stoffers B, Blankenberg S, Westermann D, Lindner D (2019) Inflammation and fibrosis in murine models of heart failure. *Basic Res Cardiol* 114:19. <https://doi.org/10.1007/s00395-019-0722-5>
- Bajpai G, Bredemeyer A, Li W, Zaitsev K, Koenig AL, Lokshina I, Mohan J, Ivey B, Hsiao HM, Weinheimer C, Kovacs A, Epelman S, Artyomov M, Kreisler D, Lavine KJ (2019) Tissue resident CCR2- and CCR2+ cardiac macrophages differentially orchestrate monocyte recruitment and fate specification following myocardial injury. *Circ Res* 124:263–278. <https://doi.org/10.1161/CIRCRESAHA.118.314028>
- Bajpai G, Schneider C, Wong N, Bredemeyer A, Hulsmans M, Nahrendorf M, Epelman S, Kreisler D, Liu Y, Itoh A, Shankar TS, Selzman CH, Drakos SG, Lavine KJ (2018) The human heart contains distinct macrophage subsets with divergent origins and functions. *Nat Med* 24:1234–1245. <https://doi.org/10.1038/s41591-018-0059-x>
- Balamurugan K, Sharan S, Klarmann KD, Zhang Y, Coppola V, Summers GH, Roger T, Morrison DK, Keller JR, Sterneck E (2013) FBXW7 α attenuates inflammatory signalling by down-regulating C/EBP δ and its target gene Tlr4. *Nat Commun* 4:1662–1662. <https://doi.org/10.1038/ncomms2677>
- Bansal SS, Ismahil MA, Goel M, Zhou G, Rokosh G, Hamid T, Prabhu SD (2019) Dysfunctional and proinflammatory regulatory T-lymphocytes are essential for adverse cardiac remodeling in ischemic cardiomyopathy. *Circulation* 139:206–221. <https://doi.org/10.1161/circulationaha.118.036065>
- Blackburn PR, Xu Z, Tumelty KE, Zhao RW, Monis WJ, Harris KG, Gass JM, Cousin MA, Boczek NJ, Mitkov MV, Cappel MA, Francomano CA, Parisi JE, Klee EW, Faqeih E, Alkuraya FS, Layne MD, McDonnell NB, Atwal PS (2018) Bi-allelic Alterations in AEBP1 lead to defective collagen assembly and connective tissue structure resulting in a variant of Ehlers-Danlos syndrome. *Am J Hum Genet* 102:696–705. <https://doi.org/10.1016/j.ajhg.2018.02.018>
- Chihara N, Madi A, Kondo T, Zhang H, Acharya N, Singer N, Nyman J, Marjanovic ND, Kowalczyk MS, Wang C, Kurtulus S, Law T, Etmnian Y, Nevin J, Buckley CD, Burkett PR, Buenrostro JD, Rozenblatt-Rosen O, Anderson AC, Regev A, Kuchroo VK (2018) Induction and transcriptional regulation of the co-inhibitory gene module in T cells. *Nature* 558:454–459. <https://doi.org/10.1038/s41586-018-0206-z>
- Choudhury RH, Dunk CE, Lye SJ, Aplin JD, Harris LK, Jones RL (2017) Extravillous trophoblast and endothelial cell crosstalk mediates leukocyte infiltration to the early remodeling decidual spiral arteriole wall. *J Immunol* 198:4115–4128. <https://doi.org/10.4049/jimmunol.1601175>
- Chung ES, Packer M, Lo KH, Fasanmade AA, Willerson JT, Anti TNFTACHFI (2003) Randomized, double-blind, placebo-controlled, pilot trial of infliximab, a chimeric monoclonal antibody to tumor necrosis factor-alpha, in patients with moderate-to-severe heart failure: results of the anti-TNF therapy against congestive heart failure (ATTACH) trial. *Circulation* 107:3133–3140. <https://doi.org/10.1161/01.CIR.0000077913.60364.D2>
- Cochain C, Vafadarnejad E, Arampatzis P, Pelisek J, Winkels H, Ley K, Wolf D, Saliba A-E, Zerneck A (2018) Single-cell RNA-Seq reveals the transcriptional landscape and heterogeneity of aortic macrophages in murine atherosclerosis. *Circ Res* 122:1661–1674. <https://doi.org/10.1161/CIRCRESAHA.117.312509>
- De Nardo D, Labzin LI, Kono H, Seki R, Schmidt SV, Beyer M, Xu D, Zimmer S, Lahrmann C, Schildberg FA, Vogelhuber J, Kraut M, Ulas T, Kerksiek A, Krebs W, Bode N, Grebe A, Fitzgerald ML, Hernandez NJ, Williams BRG, Knolle P, Kneilling M, Röcken M, Lütjohann D, Wright SD, Schultze JL, Latz E (2014) High-density lipoprotein mediates anti-inflammatory reprogramming of macrophages via the transcriptional regulator ATF3. *Nat Immunol* 15:152–160. <https://doi.org/10.1038/ni.2784>
- Dick SA, Macklin JA, Nejat S, Momen A, Clemente-Casares X, Althagafi MG, Chen J, Kantores C, Hosseinzadeh S, Aronoff L, Wong A, Zaman R, Barbu I, Besla R, Lavine KJ, Razani B, Ginhoux F, Husain M, Cybulsky MI, Robbins CS, Epelman S (2019) Self-renewing resident cardiac macrophages limit adverse remodeling following myocardial infarction. *Nat Immunol* 20:29–39. <https://doi.org/10.1038/s41590-018-0272-2>
- Farbehi N, Patrick R, Dorison A, Xaymardan M, Janbandhu V, Wystub-Lis K, Ho JW, Nordon RE, Harvey RP (2019) Single-cell expression profiling reveals dynamic flux of cardiac stromal, vascular and immune cells in health and injury. *Elife*. <https://doi.org/10.7554/eLife.43882>
- Fernandez DM, Rahman AH, Fernandez NF, Chudnovskiy A, Amir E-AD, Amadori L, Khan NS, Wong CK, Shamailova R, Hill CA, Wang Z, Remark R, Li JR, Pina C, Faries C, Awad AJ, Moss N, Björkegren JLM, Kim-Schulze S, Gnjatich S, Ma'ayan A, Mocco J, Faries P, Merad M, Giannarelli C (2019) Single-cell immune landscape of human atherosclerotic plaques. *Nat Med* 25:1576–1588. <https://doi.org/10.1038/s41591-019-0590-4>
- Finak G, McDavid A, Yajima M, Deng J, Gersuk V, Shalek AK, Slichter CK, Miller HW, McElrath MJ, Prlic M, Linsley PS, Gottardo R (2015) MAST: a flexible statistical framework for assessing transcriptional changes and characterizing heterogeneity in single-cell RNA sequencing data. *Genome Biol* 16:278–278. <https://doi.org/10.1186/s13059-015-0844-5>
- Fischer A, Schumacher N, Maier M, Sendtner M, Gessler M (2004) The Notch target genes Hey1 and Hey2 are required for embryonic vascular development. *Genes Dev* 18:901–911. <https://doi.org/10.1101/gad.291004>
- Fu X, Khalil H, Kanisicak O, Boyer JG, Vagnozzi RJ, Maliken BD, Sargent MA, Prasad V, Valiente-Alandi I, Blaxall BC, Molkentin JD (2018) Specialized fibroblast differentiated states underlie scar formation in the infarcted mouse heart. *J Clin Invest* 128:2127–2143. <https://doi.org/10.1172/jci98215>
- Gladka MM, Molenaar B, de Ruiter H, van der Elst S, Tsui H, Versteeg D, Lacraz GPA, Huijbers MMH, van Oudenaarden A, van Rooij E (2018) Single-cell sequencing of the healthy and diseased heart reveals cytoskeleton-associated protein 4 as a new modulator

- of fibroblasts activation. *Circulation* 138:166–180. <https://doi.org/10.1161/circulationaha.117.030742>
20. Ha H, Debnath B, Neamati N (2017) Role of the CXCL8-CXCR1/2 axis in cancer and inflammatory diseases. *Theranostics* 7:1543–1588. <https://doi.org/10.7150/thno.15625>
 21. He Z, Way KJ, Arikawa E, Chou E, Opland DM, Clermont A, Isshiki K, Ma RC, Scott JA, Schoen FJ, Feener EP, King GL (2005) Differential regulation of angiotensin II-induced expression of connective tissue growth factor by protein kinase C isoforms in the myocardium. *J Biol Chem* 280:15719–15726. <https://doi.org/10.1074/jbc.M413493200>
 22. Howangyin KY, Zlatanova I, Pinto C, Ngkelo A, Cochain C, Rouanet M, Vilar J, Lemitre M, Stockmann C, Fleischmann BK, Mallat Z, Silvestre JS (2016) Myeloid-epithelial-reproductive receptor tyrosine kinase and milk fat globule epidermal growth factor 8 coordinately improve remodeling after myocardial infarction via local delivery of vascular endothelial growth factor. *Circulation* 133:826–839. <https://doi.org/10.1161/circulationaha.115.020857>
 23. Hulsmans M, Sager HB, Roh JD, Valero-Munoz M, Houstis NE, Iwamoto Y, Sun Y, Wilson RM, Wojtkiewicz G, Tricot B, Osborne MT, Hung J, Vinegoni C, Naxerova K, Sosnovik DE, Zile MR, Bradshaw AD, Liao R, Tawakol A, Weissleder R, Rosenzweig A, Swirski FK, Sam F, Nahrendorf M (2018) Cardiac macrophages promote diastolic dysfunction. *J Exp Med* 215:423–440. <https://doi.org/10.1084/jem.20171274>
 24. Imura A, Hori T, Imada K, Ishikawa T, Tanaka Y, Maeda M, Imamura S, Uchiyama T (1996) The human OX40/gp34 system directly mediates adhesion of activated T cells to vascular endothelial cells. *J Exp Med* 183:2185–2195. <https://doi.org/10.1084/jem.183.5.2185>
 25. Jaitin DA, Adlung L, Thaiss CA, Weiner A, Li B, Descamps H, Lundgren P, Blieriot C, Liu Z, Deczkowska A, Keren-Shaul H, David E, Zmora N, Eldar SM, Lubezky N, Shibolet O, Hill DA, Lazar MA, Colonna M, Ginhoux F, Shapiro H, Elinav E, Amit I (2019) Lipid-associated macrophages control metabolic homeostasis in a Trem2-dependent manner. *Cell* 178:686–698.e614. <https://doi.org/10.1016/j.cell.2019.05.054>
 26. Keren-Shaul H, Spinrad A, Weiner A, Matcovitch-Natan O, Dvir-Szternfeld R, Ulland TK, David E, Baruch K, Lara-Astaiso D, Toth B, Itzkovitz S, Colonna M, Schwartz M, Amit I (2017) A unique microglia type associated with restricting development of Alzheimer's disease. *Cell* 169:1276–1290.e1217. <https://doi.org/10.1016/j.cell.2017.05.018>
 27. Kocher AA, Schuster MD, Szabolcs MJ, Takuma S, Burkhoff D, Wang J, Homma S, Edwards NM, Itescu S (2001) Neovascularization of ischemic myocardium by human bone-marrow-derived angioblasts prevents cardiomyocyte apoptosis, reduces remodeling and improves cardiac function. *Nat Med* 7:430–436. <https://doi.org/10.1038/86498>
 28. Kumar BV, Ma W, Miron M, Granot T, Guyer RS, Carpenter DJ, Senda T, Sun X, Ho SH, Lerner H, Friedman AL, Shen Y, Farber DL (2017) Human tissue-resident memory t cells are defined by core transcriptional and functional signatures in lymphoid and mucosal sites. *Cell Rep* 20:2921–2934. <https://doi.org/10.1016/j.celrep.2017.08.078>
 29. Lachmann A, Giorgi FM, Lopez G, Califano A (2016) ARACNe-AP: gene network reverse engineering through adaptive partitioning inference of mutual information. *Bioinformatics* 32:2233–2235. <https://doi.org/10.1093/bioinformatics/btw216>
 30. Li J, Diao B, Guo S, Huang X, Yang C, Feng Z, Yan W, Ning Q, Zheng L, Chen Y, Wu Y (2017) VSIG4 inhibits proinflammatory macrophage activation by reprogramming mitochondrial pyruvate metabolism. *Nat Commun* 8:1322–1322. <https://doi.org/10.1038/s41467-017-01327-4>
 31. Li J, Yang KY, Tam RYC, Chan VW, Lan HY, Hori S, Zhou B, Lui KO (2019) Regulatory T-cells regulate neonatal heart regeneration by potentiating cardiomyocyte proliferation in a paracrine manner. *Theranostics* 9:4324–4341. <https://doi.org/10.7150/thno.32734>
 32. Li Z, Solomonidis EG, Meloni M, Taylor RS, Duffin R, Dobie R, Magalhaes MS, Henderson BEP, Louwe PA, D'Amico G, Hodi-vala-Dilke KM, Shah AM, Mills NL, Simons BD, Gray GA, Henderson NC, Baker AH, Brittan M (2019) Single-cell transcriptome analyses reveal novel targets modulating cardiac neovascularization by resident endothelial cells following myocardial infarction. *Eur Heart J*. <https://doi.org/10.1093/eurheartj/ehz305>
 33. Liao X, Sharma N, Kapadia F, Zhou G, Lu Y, Hong H, Paruchuri K, Mahabeleshwar GH, Dalmas E, Venteclef N, Flask CA, Kim J, Doreian BW, Lu KQ, Kaestner KH, Hamik A, Clément K, Jain MK (2011) Krüppel-like factor 4 regulates macrophage polarization. *J Clin Invest* 121:2736–2749. <https://doi.org/10.1172/JCI45444>
 34. Litviňuková M, Talavera-López C, Maatz H, Reichart D, Worth CL, Lindberg EL, Kanda M, Polanski K, Heinig M, Lee M, Nadelmann ER, Roberts K, Tuck L, Fasouli ES, DeLaughter DM, McDonough B, Wakimoto H, Gorham JM, Samari S, Mahbubani KT, Saeb-Parsy K, Patone G, Boyle JJ, Zhang H, Zhang H, Viveiros A, Oudit GY, Bayraktar O, Seidman JG, Seidman CE, Noseda M, Hubner N, Teichmann SA (2020) Cells of the adult human heart. *Nature*. <https://doi.org/10.1038/s41586-020-2797-4>
 35. Liu X, Wang Y, Lu H, Li J, Yan X, Xiao M, Hao J, Alekseev A, Khong H, Chen T, Huang R, Wu J, Zhao Q, Wu Q, Xu S, Wang X, Jin W, Yu S, Wang Y, Wei L, Wang A, Zhong B, Ni L, Liu X, Nurieva R, Ye L, Tian Q, Bian X-W, Dong C (2019) Genome-wide analysis identifies NR4A1 as a key mediator of T cell dysfunction. *Nature* 567:525–529. <https://doi.org/10.1038/s41586-019-0979-8>
 36. Martin JC, Chang C, Boschetti G, Ungaro R, Giri M, Grout JA, Gettler K, Chuang L-S, Nayar S, Greenstein AJ, Dubinsky M, Walker L, Leader A, Fine JS, Whitehurst CE, Mbow ML, Kugathasan S, Denson LA, Hyams JS, Friedman JR, Desai PT, Ko HM, Laface I, Akturk G, Schadt EE, Salmon H, Gnjjatic S, Rahman AH, Merad M, Cho JH, Kenigsberg E (2019) Single-cell analysis of Crohn's disease lesions identifies a pathogenic cellular module associated with resistance to anti-TNF therapy. *Cell* 178:1493–1508.e1420. <https://doi.org/10.1016/j.cell.2019.08.008>
 37. Nakajima T, Schulte S, Warrington KJ, Kopecky SL, Frye RL, Goronzy JJ, Weyand CM (2002) T-cell-mediated lysis of endothelial cells in acute coronary syndromes. *Circulation* 105:570–575. <https://doi.org/10.1161/hc0502.103348>
 38. Nevers T, Salvador AM, Velazquez F, Ngwenyama N, Carrillo-Salinas FJ, Aronovitz M, Blanton RM, Alcaide P (2017) Th1 effector T cells selectively orchestrate cardiac fibrosis in non-ischemic heart failure. *J Exp Med* 214:3311–3329. <https://doi.org/10.1084/jem.20161791>
 39. Oka T, Akazawa H, Naito AT, Komuro I (2014) Angiogenesis and cardiac hypertrophy: maintenance of cardiac function and causative roles in heart failure. *Circ Res* 114:565–571. <https://doi.org/10.1161/circresaha.114.300507>
 40. Palethorpe HM, Tomita Y, Smith E, Pei JV, Townsend AR, Price TJ, Young JP, Yool AJ, Hardingham JE (2018) The aquaporin 1 inhibitor Bacopaside II reduces endothelial cell migration and tubulogenesis and induces apoptosis. *Int J Mol Sci*. <https://doi.org/10.3390/ijms19030653>
 41. Ramachandran P, Dobie R, Wilson-Kanamori JR, Dora EF, Henderson BEP, Luu NT, Portman JR, Matchett KP, Brice M, Marwick JA, Taylor RS, Efreмова M, Vento-Tormo R, Carragher NO, Kendall TJ, Fallowfield JA, Harrison EM, Mole DJ, Wigmore SJ, Newsome PN, Weston CJ, Iredale JP, Tacke F, Pollard JW, Ponting CP, Marioni JC, Teichmann SA, Henderson NC (2019)

- Resolving the fibrotic niche of human liver cirrhosis at single-cell level. *Nature*. <https://doi.org/10.1038/s41586-019-1631-3>
42. Rodriguez P, Sassi Y, Troncone L, Benard L, Ishikawa K, Gordon RE, Lamas S, Laborda J, Hajjar RJ, Lebeche D (2019) Deletion of delta-like 1 homologue accelerates fibroblast-myofibroblast differentiation and induces myocardial fibrosis. *Eur Heart J* 40:967–978. <https://doi.org/10.1093/eurheartj/ehy188>
 43. Russo RC, Garcia CC, Teixeira MM, Amaral FA (2014) The CXCL8/IL-8 chemokine family and its receptors in inflammatory diseases. *Expert Rev Clin Immunol* 10:593–619. <https://doi.org/10.1586/1744666X.2014.894886>
 44. Sager HB, Hulsmans M, Lavine KJ, Moreira MB, Heidt T, Courties G, Sun Y, Iwamoto Y, Tricot B, Khan OF, Dahlman JE, Borodovsky A, Fitzgerald K, Anderson DG, Weissleder R, Libby P, Swirski FK, Nahrendorf M (2016) Proliferation and recruitment contribute to myocardial macrophage expansion in chronic heart failure. *Circ Res* 119:853–864. <https://doi.org/10.1161/CIRCRESAHA.116.309001>
 45. Schalper KA, Carleton M, Zhou M, Chen T, Feng Y, Huang SP, Walsh AM, Baxi V, Pandya D, Baradet T, Locke D, Wu Q, Reilly TP, Phillips P, Nagineni V, Gianino N, Gu J, Zhao H, Perez-Gracia JL, Sanmamed MF, Melero I (2020) Elevated serum interleukin-8 is associated with enhanced intratumor neutrophils and reduced clinical benefit of immune-checkpoint inhibitors. *Nat Med* 26:688–692. <https://doi.org/10.1038/s41591-020-0856-x>
 46. Schwab SR, Cyster JG (2007) Finding a way out: lymphocyte egress from lymphoid organs. *Nat Immunol* 8:1295–1301. <https://doi.org/10.1038/ni1545>
 47. Shen L, Jhund PS, Petrie MC, Claggett BL, Barlera S, Cleland JGF, Dargie HJ, Granger CB, Kjekshus J, Kober L, Latini R, Maggioni AP, Packer M, Pitt B, Solomon SD, Swedberg K, Tavazzi L, Wikstrand J, Zannad F, Zile MR, McMurray JJV (2017) Declining risk of sudden death in heart failure. *N Engl J Med* 377:41–51. <https://doi.org/10.1056/NEJMoa1609758>
 48. Shetelig C, Limalanathan S, Hoffmann P, Seljeflot I, Gran JM, Eritsland J, Andersen G (2018) Association of IL-8 with infarct size and clinical outcomes in patients with STEMI. *J Am Coll Cardiol* 72:187–198. <https://doi.org/10.1016/j.jacc.2018.04.053>
 49. Skelly DA, Squiers GT, McLellan MA, Bolisetty MT, Robson P, Rosenthal NA, Pinto AR (2018) Single-cell transcriptional profiling reveals cellular diversity and intercommunication in the mouse heart. *Cell Rep* 22:600–610. <https://doi.org/10.1016/j.celrep.2017.12.072>
 50. Swirski FK, Nahrendorf M (2013) Leukocyte behavior in atherosclerosis, myocardial infarction, and heart failure. *Science* 339:161–166. <https://doi.org/10.1126/science.1230719>
 51. Tucker NR, Chaffin M, Fleming SJ, Hall AW, Parsons VA, Bedi KC Jr, Akkad AD, Herndon CN, Arduini A, Papangeli I, Roselli C, Aguet F, Choi SH, Ardlie KG, Babadi M, Margulies KB, Stegmann CM, Ellinor PT (2020) Transcriptional and cellular diversity of the human heart. *Circulation*. <https://doi.org/10.1161/circulationaha.119.045401>
 52. Vento-Tormo R, Efremova M, Botting RA, Turco MY, Vento-Tormo M, Meyer KB, Park JE, Stephenson E, Polanski K, Goncalves A, Gardner L, Holmqvist S, Henriksson J, Zou A, Sharkey AM, Millar B, Innes B, Wood L, Wilbrey-Clark A, Payne RP, Ivarsson MA, Lisgo S, Filby A, Rowitch DH, Bulmer JN, Wright GJ, Stubbington MJT, Haniffa M, Moffett A, Teichmann SA (2018) Single-cell reconstruction of the early maternal-fetal interface in humans. *Nature* 563:347–353. <https://doi.org/10.1038/s41586-018-0698-6>
 53. Wang L, Yu P, Zhou B, Song J, Li Z, Zhang M, Guo G, Wang Y, Chen X, Han L, Hu S (2020) Single-cell reconstruction of the adult human heart during heart failure and recovery reveals the cellular landscape underlying cardiac function. *Nat Cell Biol* 22:108–119. <https://doi.org/10.1038/s41556-019-0446-7>
 54. Wherry EJ, Kurachi M (2015) Molecular and cellular insights into T cell exhaustion. *Nat Rev Immunol* 15:486–499. <https://doi.org/10.1038/nri3862>
 55. You LR, Lin FJ, Lee CT, DeMayo FJ, Tsai MJ, Tsai SY (2005) Suppression of Notch signalling by the COUP-TFII transcription factor regulates vein identity. *Nature* 435:98–104. <https://doi.org/10.1038/nature03511>
 56. Zhang L, Yu X, Zheng L, Zhang Y, Li Y, Fang Q, Gao R, Kang B, Zhang Q, Huang JY, Konno H, Guo X, Ye Y, Gao S, Wang S, Hu X, Ren X, Shen Z, Ouyang W, Zhang Z (2018) Lineage tracking reveals dynamic relationships of T cells in colorectal cancer. *Nature* 564:268–272. <https://doi.org/10.1038/s41586-018-0694-x>